scientific reports

Check for updates

OPEN

Electrocapacitive removal of Na and Cd ions from contaminated aqueous solution using Fe_3O_4-poly (3,4-ethylenedioxythiophene) poly(styrene sulfonate) modified chitosan nanosheets

Oluwaseyi D. Saliu[1,2]✉, Omphemetse Leping[1], Tunde L. Yusuf[4], Adewale G. Adeniyi[3] & James Ramontja[1]✉

Chitosan nanosheets (NS) stabilized on poly (3,4-ethylenedioxythiophene): poly(styrene sulfonate) (PEDOT: PSS) was functionalized using Fe_3O_4 to capacitively remove chloride ions and toxic cadmium ions at optimized pH, concentration, and number of charging cycles. The synthesis procedure was investigated by Fourier transform infrared spectroscopy (FTIR), X-Ray Diffractometer (XRD), Transmission Electron Microscope (TEM), Scanning Electron Microscope – Energy Dispersive X-ray Spectroscopy (SEM-EDS), and Brunauer-Emmett-Teller (BET). The analyses confirms increase in surface area of the nanocomposite from 41 to 132 m^2/g and a decrease in crystallinity from 75.3 to 66.9% after nanosheet formation. The highest sorption exchange capacity (SEC) for this work, 93% $CdCO_3$ removal is achieved at 100 CDI cycles while 82% NaCl removal was achieved at 80 cycles. The SEC% increased with pH during Na ion deionization and decreased with pH during Cd removal. The works shows that chitosan is able to impart advanced structural properties to Fe_3O_4 and PEDOT and is able to reduce reverse migration of ions from electrodes to bulk solution, leading to higher SEC performance.

Keywords Capacitive deionization, desalination, PEDOT, salt removal, nanocomposites

The United Nations have acknowledged clean water as a basic human right for all, but 70% people globally do not have access to it[1], and with the rapidly increasing human population, it is reported that by 2025, 86% of the population around the world will be affected by water scarcity[2]. There is approximately 1.386 billion km^3 of water on Earth, of which 2.5% is fresh water and 97.5% is salt water[3]. Saltwater accounts for the vast majority of water on the earth, thus many desalination processes have been used in an effort to generate more clean water, as its affordability and availability are critical for the social and economic growth of the twenty-first century. Heavy metal ions dissolved in water are harmful to both the environment and humans, and their accumulation in the food chain can lead to catastrophic diseases[4]. Heavy metal ion poisoning is caused by a variety of circumstances, including the quantity, type of contact, chemical composition, and nutritional state of the exposed individuals[5]. Cadmium and lead heavy metal poisoning can result in disorders such as high blood pressure, kidney damage, testicular tissue destruction, osteoporosis, and red blood cell destruction[6,7]. nutrients, pathogens, plastics, pesticides, and heavy metals into the water[8]. Generally, cadmium pollution is caused by the following industries: steel electroplating[9], the production of electronic and electric systems, phosphate fertilizers production, nuclear reactors and the production of stabilizers[10].

[1]Energy, Sensors and Multifunctional Nanomaterials Research Group, Department of Chemical Sciences, University of Johannesburg, Doornfontein, PO Box 17011, Johannesburg 2028, South Africa. [2]Department of Industrial Chemistry, University of Ilorin, Ilorin, Nigeria. [3]Chemical Engineering Department, Faculty of Engineering and Technology, University of Ilorin, P.M.B. 1515, Ilorin, Nigeria. [4] Department of Chemistry, Faculty of Natural and Agricultural Sciences, University of Pretoria, Private Bag X20, Hatfield 0028, Pretoria, South Africa. ✉email: saliu3@uic.edu; jamesr@uj.ac.za

Just as cadmium carbonate problems exists naturally, so does sodium chloride, this salt exists naturally in seawater and its salinity ranges between 24 000 and 42 000 ppm[10], and thus is a primary agent that causes hardness of water. Consequently, capacitive deionization (CDI) technique has been employed to remove halide ions in water (sorption rates: 20–65%), to remove heavy metals from water (sorption rates: 40–99%; highest for chromium and lead), to treat hardness of water (sorption rates: < 50%; lowest for sodium ions). Other methods employed for water treatment includes nanofiltration, reverse osmosis, ion exchange, multi-effect distillation, electrodialysis. CDI's main advantage is that it can successfully desalinate water without consuming high amount energy, this is possible since it does not require the use of high pressure. It is a very selective method and does not require the pretreatment of effluents before desalination, and it is also highly scalable. CDI is a robust and novel electrochemical technique employed for the desalination of water by using an electrical double layer[11]. It achieves this by adsorbing the positive ions from salt water onto the electric double layer (EDL) of two porous electrodes (like activated carbon, transition metal oxides and carbides, polymer-metal oxides composites etc.) whilst using a minimal electrical field of 0.6–1.5 V[12].

The incorporation of magnetite into polymeric nanocomposites are anticipated to capacitively deionise salts from seawater[13]. Functional monomers are gradually gaining prominence, and many copolymers containing reactive functional groups are currently being synthesized for water applications. These functional groups give a way to polymer modification for specific end applications. Poly (3,4-ethylenedioxythiophene) polystyrene sulfonate often used for the deposition of magnetic nanoparticles, is a good biocompatible conductive polymer due to its hydrophilic nature and low toxicity. In addition, reactive groups in the main chain structure of PEDOT allow for additional functionalization[14]. Chitosan has been widely researched for adsorption and deionization applications due to its amino and hydroxyl groups that have good affinity for binding to metal[15]. Biopolymers function in conjunction with divalent metal ions, such as calcium, to aid the production and stabilization of sludge flocs in both aerobic and anaerobic treatment systems[15,16]. This makes it possible to cleanly separate the biomass from the liquid phase. Wastewater treatment frequently makes use of biopolymers.

Previous works have prepared fly ash-coated chitosan blends to remove Cu, Zn, and As, showing an adsorption capacity of 28.65 mg/ g, 55.52 mg/g, and 19.10 mg/g, other works have formed composites of chitosan and other biopolymers like poly(vinyl alcohol), to complement its poor solvent incompatibilities[17,18]. In this work, we designed a composite of chitosan and PEDOT, then functionalize it with Fe_3O_4 NPs to give a synergistic effect, producing a flexible, low-cost, and light weight electrode material for CDI[19]. The aromatic rings in PEDOT units can undergo π-π stacking interactions with the surface of Fe3O4 nanoparticles. This interaction further stabilizes the nanocomposite structure and promotes the uniform dispersion of Fe3O4 within the polymer matrix. This research looks at designing a nanocomposite consisting of the magnetite, PEDOT: PSS and chitosan for the capacitive deionisation of NaCl and $CdCO_3$ from saline water, where the chitosan is able to drive higher SEC values by reducing reverse migration of ions back to the bulk solution after CDI.

Materials and methods

Materials

$FeCl_3.6H_2O$, acetic acid, chitosan, ammonium hydroxide solution, PEDOT: PSS, DMSO, PVA, Ethanol and NaCl were purchased from Sigma Aldrich. $FeCl_2.4H_2O$, nickel foam, nafion, and oxalic acid were purchased from Alfar Aeser, the KJ Group, microfiltration (pty) Ltd, and Merck, respectively.

Preparation of iron oxide magnetic nanoparticles

Iron oxide nanoparticles were prepared via the co-precipitation method[19]. In a typical procedure, 6.74 g $FeCl_3.6H_2O$ and 3.35 g $FeCl_2.4H_2O$ were dissolved in 100 ml deionized water on a stir bar at a speed of 300 rpm and a temperature of 50 °C. Nitrogen gas was introduced to the reaction vessel followed by the dropwise addition of 16.67 ml ammonia solution (25%) into the vessel and the speed was increased to 500 rpm and temperature to 80 °C. After the addition of ammonia solution, the colour of the solution immediately changed from orange to black. Stirring continued at 80 °C for 2 h. The synthesized magnetite was washed three times with deionized water and once with ethanol and collected by a permanent magnet. The product was dried at 80 °C in an oven for 26 h.

Preparation of the Fe3O4@PEDOT: PSS nanocomposite

Fe_3O_4@PEDOT: PSS nanocomposite was prepared using the in- situ impregnation method. Briefly, 0.01 g Fe_3O_4 nanoparticles were dissolved in 1 ml of PEDOT: PSS solution. The obtained mixture was vortexed for 10 min and stored at 4 °C overnight[18]. The solution was placed on a watch glass and dried in a cupboard for 72 h.

Preparation of Fe3O4@PEDOT: PSS modified chitosan nanosheets

For the preparation of Fe_3O_4@PEDOT: PSS modified chitosan nanosheets, 100 ml of deionised water was added to a 250 ml round bottom flask. This was followed by the addition of 0.5 g chitosan, 0.1 g poly vinyl alcohol (PVA) and 5 ml of 0.2% acetic acid. The solution was stirred for 24 h at 25 °C[20]. For the synthesis of the nanosheet, 100 mg of the Fe_3O_4@PEDOT: PSS nanocomposite was added to 40 ml dq1imethyl sulfoxide (DMSO) in a 100 ml beaker and the mixture was sonicated for 2 h. Thereafter, 20 ml of the nanocomposite solution was added to the chitosan and PVA, and the mixture was stirred for 24 h. The obtained nanosheets were dried at 50 °C in a vacuum oven for 48 h, to be used as negative electrodes in CDI process.

Preparation of CDI electrodes

The negative electrode was prepared by cutting out 19 mm circumference of nickel foam using the $KENNEDY$ 518–1589 and a hammer, this was followed by flattening the nickel foam using the heat press machine. The Fe_3O_4@PEDOT: PSS nanocomposite and Fe_3O_4@PEDOT: PSS modified chitosan nanosheets were respectively

placed on the nickel foam using nafion to yield the negative electrode followed by heat pressing to make the electrode uniform. Each of the CDI electrodes were prepared by mixing 80% of each nanocomposite and nanosheet as active materials, 10% of carbon black, and 10% of PVDF binder. The mixture was then added with 20 mL of ethanol and agitated to achieve homogeneity until a dough-like paste formed. The paste was pressed to the required thickness (0.1 mm), cut into 50 × 50 mm pieces, and dried in a vacuum oven at 50 °C overnight. Finally, the electrodes were tested for CDI applications. The capacitive sodium and cadmium removal experiments were carried out in a batch mode in a laboratory-scale CDI reactor. A solution tank, a peristaltic pump, a pair of electrodes, an electrochemical workstation potentiostat (equipped with Gamry software), and digital conductivity meter were all part of the CDI system. Two identical electrodes were assembled into a self-made CDI cell where 30 mL of 100 ppm sodium chloride and cadmium chloride solution were pumped with a peristaltic pump into the cell. A flow rate of 20 $mLmin^{-1}$ and a potential of 1.2 V was employed, the effect of pH, concentration and cycles time were investigated[37,38].

Results and discussions

The FTIR was employed to confirm the functional groups in the nanocomposite and the nanosheet. Firstly, in Fig. 1a, the FTIR confirmed successful synthesis of Fe_3O_4 nanoparticles. The pronounced medium band at around 587 cm^{-1} is characteristic of the Fe-O bond and it confirms the formation of magnetic nanoparticles. The intensely broad bands at 3406 cm^{-1} and 3143 cm^{-1} are attributed to the stretching of -OH and NH_2, respectively; while the band at around 1624 cm^{-1} is attributed to -OH bending[21]. The stretching vibrations of the -CO group can be seen at the band at 1396 cm^{-1}[22]. The pronounced medium band at around 587 cm^{-1} is characteristic of the Fe-O bond and it confirms the formation of magnetic nanoparticles[21]. The synthesis of Fe_3O_4@PEDOT: PSS nanocomposite was confirmed in Fig. 1b. The phenyl side group and quinoid PEDOT and the hydroxyl stretching is seen at broad bands of 3427 cm^{-1} and 3406 cm^{-1}, respectively, while amine stretching is seen at a broad band of 3143 cm^{-1}. Hydroxyl also shows bending at 1638 cm^{-1}[21].

At around 1638 cm^{-1} is the stretching of C = C quinoid PEDOT and phenyl side group, the C-C stretching of the thiophene ring is observed at approximately 1396 cm^{-1}, around 1120 cm^{-1} is the stretching of SO_3H groups and S-OH molecules associated with PSS[23]. Lastly, the peak at 623 cm^{-1} which shifted upward from the nanoparticles spectra and is characteristic of Fe-O, confirmed the successful synthesis of the nanocomposite. This band is more protruding in the iron oxide nanoparticles spectrum and it can also be seen in the nanocomposite spectrum at 623 cm^{-1} but is not as defined which indicates that the conductivity of PEDOT: PSS reduced the magnetism of the iron oxide nanoparticles. The formation of Fe_3O_4@PEDOT: PSS modified chitosan nanosheets was also confirmed using FTIR (see Fig. 1c). The spectrum in Fig. 2c shows intense broad peaks at 3349 cm^{-1} and 3307 cm^{-1} indicating the hydroxyl and the amine groups, respectively.

The presence of methylene ($-CH_2$) is seen with the peak at 2874 cm^{-1}[22]. The band at 1646 cm^{-1} showed the presence of N-acetyl residues[24]. The hydroxyl group of chitosan can be seen with the intensely low peak at 1425 cm^{-1}[22]. The stretching vibrations of the -CO group can be seen at the band at 1369 cm^{-1}[23]. The band at 1025 cm^{-1} is attributed to the stretching of the carbonyl group. The intensely low band at 1369 cm^{-1} on the modified chitosan nanosheet and the intensely strong bands at 1396 cm^{-1} on the nanoparticles and nanocomposite shows the integration of all three materials. The nanosheet showed very high transmittance between 80 and 100%, while the starting materials transmitted between 0 and 100%.

XRD confirmed the formation of Fe_3O_4 nanoparticles, the Fe_3O_4-PEDOT nanocomposite and the Fe_3O_4-PEDOT-chitosan nanosheet. Formation of the NPs is depicted in Fig. 1d where the 2θ values at $30.07°$, $35.41°$, $43.09°$, 53.58° and $56.06°$ correspond to the following miller indices [220], [311], [400], [422], and [511], respectively. These are characteristic of the mesoporous Fe_3O_4 nanoparticles according to the JCPDS file number (19-0629) for magnetite[25]. The intense peak at $2\theta = 35.41°$ is characteristic for the crystallinity of the Fe_3O_4 NPs. The broad peak at $2\theta = 25.70°$ in Fig. 1e shows the presence of the amorphous PEDOT: PSS and the rest of the peaks are characteristic of Fe_3O_4 nanoparticles[26] which confirmed the formation of the nanocomposite. The amorphous nature of chitosan is depicted by the peak at $2\theta = 20.37°$ in Fig. 1f and the rest of the peaks show the presence of PEDOT: PSS and Fe_3O_4 NPs.

The crystallite size tells us the exact size of the respective nanomaterial, d-spacing gives interatomic spacing between successive atoms, and the percentage intensity tells us the level of crystallinity. It was observed in Table 1, that the crystallinity of magnetite decreased from 79.89 to 75.39% in the nanocomposite and further decreased to 66.91% in the nanosheet. In addition, the size of the Fe_3O_4 NPs decreased when the respective polymers were added and this was caused by the agglomeration of the polystyrene sulfonate and amide groups in chitosan for the nanocomposite (NC) and nanosheet (NS) respectively. Lastly, the d-spacing values of the NPs and NS were found to be 0.26 Å and that of the NC was 0.24 Å; this shows that the spaces between the respective atoms were practically uniform.

TEM analysis which tells us about the internal morphology of materials confirmed the formation of NPs, NC, and NS. Figure 3a shows well dispersed Fe_3O_4 nanoparticles with no agglomeration averaging approximately 16 nm[27], which is in agreement with the size obtained (15.41 nm), see Table 1. However, the magnetic nanoparticles were agglomerated on the PEDOT: PSS in Fig. 3b and this is caused by the interactions between the particles' magneto-dipoles and the emulsification of the polystyrene sulfonate, this thus confirmed the formation of the Fe_3O_4@PEDOT: PSS nanocomposite[28]. Figure 3c shows the formation of stacked sheets with lattice fringes, indicating the presence of the nanoparticles, and this confirmed the combination of the polymers with magnetite. Furthermore, the size reduction of magnetic nanoparticles reduces their magnetism[29] and this was expected since FTIR showed that the conductivity of PEDOT: PSS reduces the magnetism of the iron oxide nanoparticles, and this was also confirmed in XRD by calculating the percentage crystallinity of the all three materials. We anticipate that the reduction in magnetism of Fe_3O_4 NPs will reduce the reverse migration of

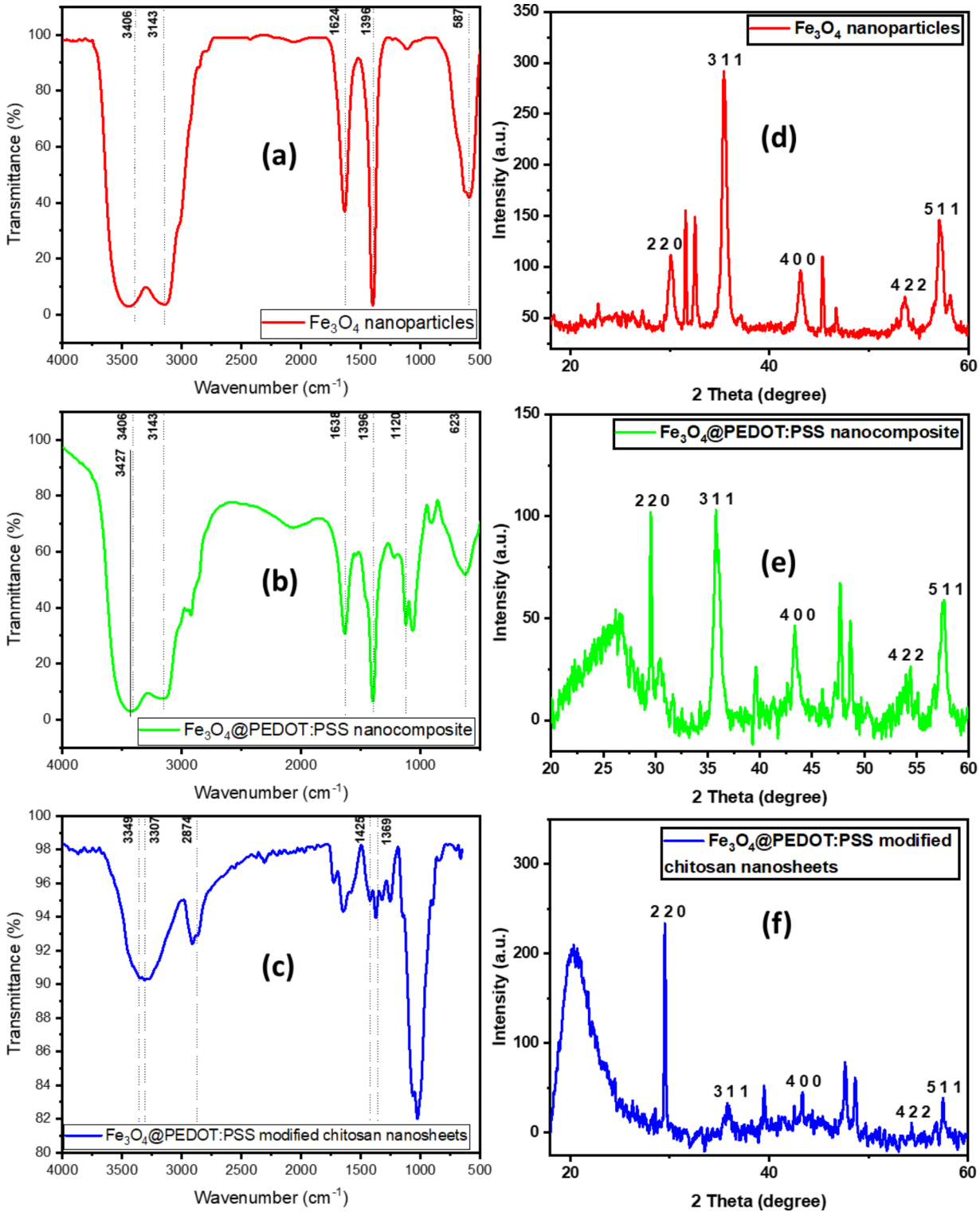

Fig. 1. (**a, b, c**) FTIR spectra of Fe_3O_4 nanoparticles, Fe_3O_4-PEDOT: PSS nanocomposite and Fe_3O_4-PEDOT: PSS modified chitosan nanosheet (**d, e, f**) XRD spectra of Fe_3O_4 nanoparticles, Fe_3O_4-PEDOT: PSS nanocomposite and Fe_3O_4-PEDOT: PSS modified chitosan nanosheet.

ions back to bulk solution after CDI processes, since magnetism is a major factor that opposes the successful accumulation of ions in the EDLC layers of CDI electrodes [29].

SEM-EDX confirmed the surface morphology of the materials which correlated with the TEM images where we saw that the nanoparticles were well dispersed, and that the addition of the conductive polymer agglomerated the nanoparticles as well as adding the biopolymer to the nanocomposite. Figure 3d shows that the NPs are

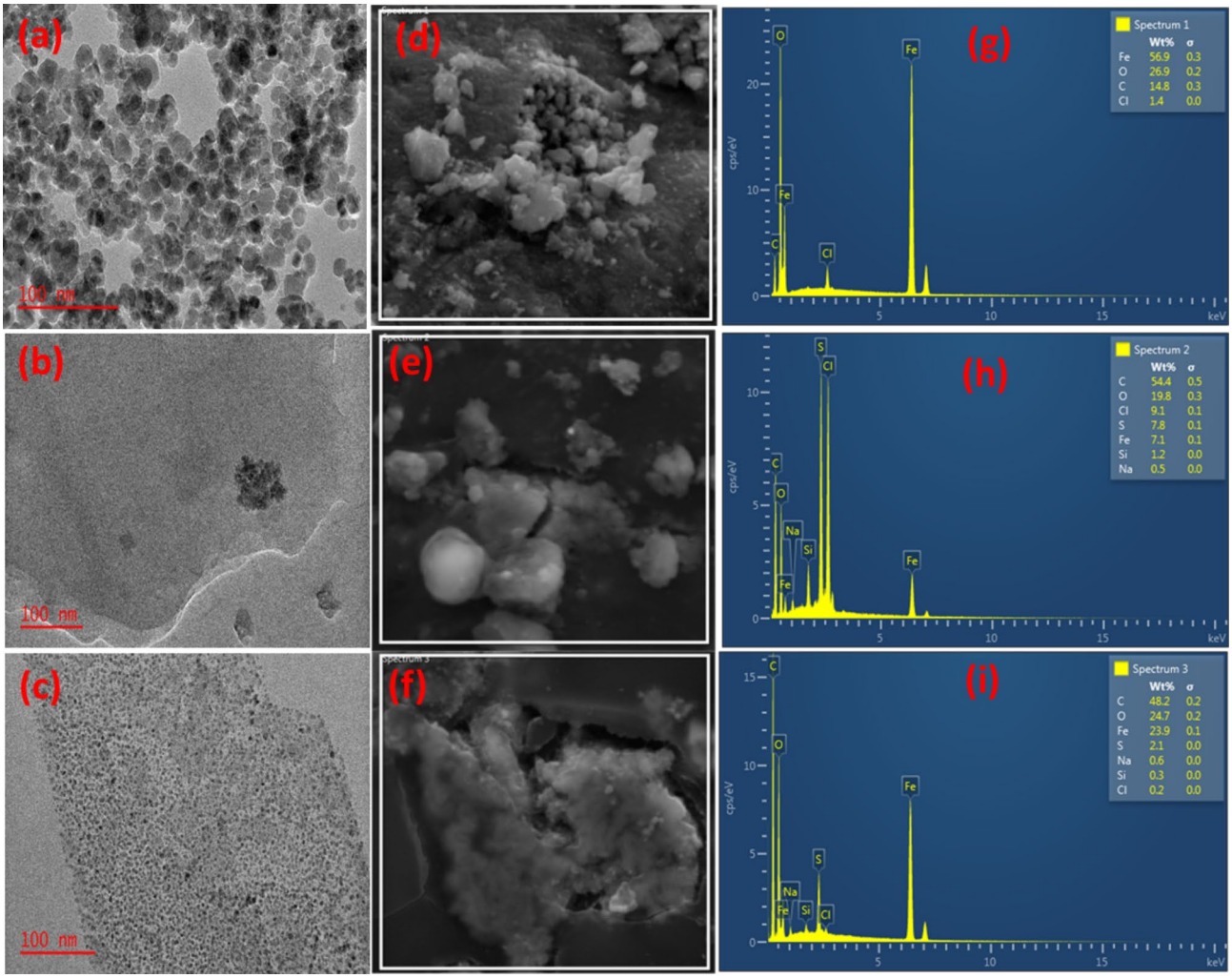

Fig. 2. Adsorption and desorption isotherms of (**a**) Fe_3O_4 nanoparticles, (**b**) Fe_3O_4@PEDOT: PSS nanocomposite, (**c**) Fe_3O_4@PEDOT: PSS modified chitosan nanosheet, and (**d**) pore size distribution of all the materials.

Samples	Crystallite size (nm)	D-spacing (Å)	Percentage crystallinity (%)
Fe_3O_4NP	15.41	0.26	79.89
Fe_3O_4@PEDOT: PSS NC	6.63	0.24	75.39
Fe_3O_4@PEDOT: PSS m-chitosan NS	7.13	0.26	66.91

Table 1. XRD parameters for the nanocomposite and nanosheet.

evenly distributed on the surface and the EDX shows all the precursors used in the synthesis of magnetite, namely, iron, chloride, and oxygen. The carbon present is the carbon tape used for analysis, and the iron and oxygen elements have high intensities confirming the formation of iron oxide. Figure 3e depicts that the iron oxide nanoparticles agglomerated on the surface of PEDOT: PSS nanocomposite as well as on the nanosheet (see Fig. 3f). This agglomeration was caused by the dispersion of PSS from the conductive polymer and -NH_2 from the biopolymer, and this further decreased the crystallinity of the m-chitosan nanosheet but increased the size of the NPs by a few nanometres from the NC, from 6.63 nm to 7.13 nm which is a difference of 0.50 nm and is therefore more or less the same (Fig. 3g and h). The formation of the NS was further confirmed by the EDX in Fig. 3i which had the following elements: C, O, S, Cl and Fe; with carbon possessing a high intensity, sulphur decreasing its intensity and the intensity of Fe further decreasing which means the material was now amorphous and this confirms the first ever successful formation of Fe_3O_4@PEDOT: PSS modified chitosan nanosheets .

BET analysis tells us about the surface area, pore sizes and pore volumes of the nanomaterials. In Fig. 2a, the adsorption-desorption isotherm is known as type IV which is characteristic of mesopores[30]. The relative pressure between 0.0 and 0.4 depicts the presence of small mesopores and capillary condensation in mesopores

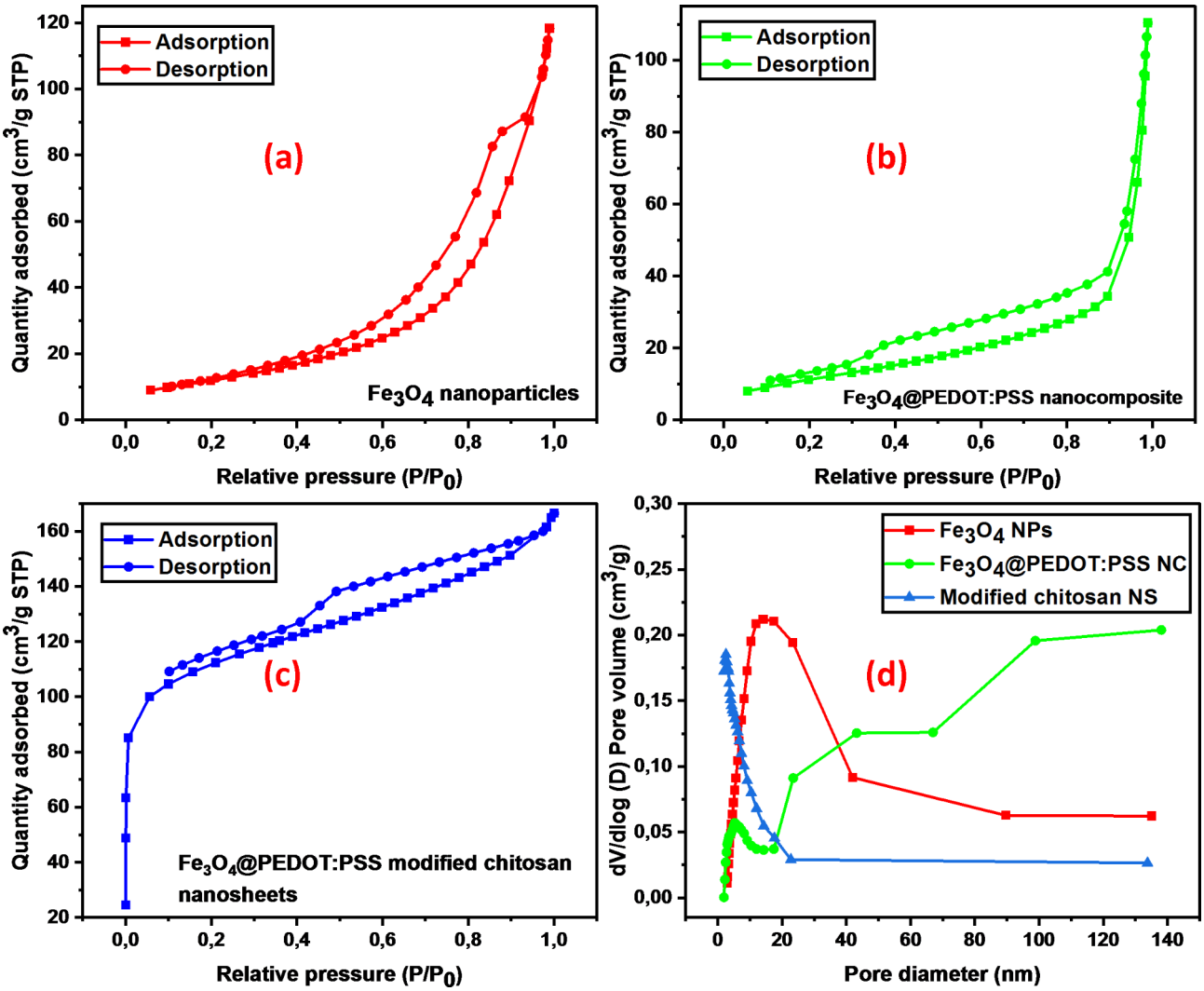

Fig. 3. (**a, b,c**) TEM images (**d, e, f**) SEM images (**g, h, i**) EDX of Fe_3O_4 nanoparticles, Fe_3O_4@PEDOT: PSS nanocomposite and Fe_3O_4@PEDOT: PSS modified chitosan nanosheet respectively.

Sample	Surface area (m^2/g)	Pore size (nm)	Pore volume (cm^3/g)
Fe_3O_4NPs	44.33	16.51	0.18
Fe_3O_4@PEDOT: PSS NC	41.89	16.30	0.17
Fe_3O_4@PEDOT: PSS m-chitosan nanosheets	132.22	0.003	0.09

Table 2. Summary of the BET results for the synthesized nanomaterials.

is seen on the hysteresis. The isotherm in Fig. 2b is also identified as type IV. It also started showing small mesopores and capillary condensation at 0.9 P/P_0. Figure 2c, which represents the m-chitosan nanosheets is identified as type I and IV. The initial step had a steep because of very strong adsorption, and this is characteristic to micropores (type I), and a slope started to form in the middle of the isotherm which depicts formation of multilayers. Figure 2d shows the BJH pore size distribution curves. Magnetite nanoparticles had a pore volume of 0.18 cm^2/g and a pore size of 16.51 nm, see Table 2. The addition of the conductive polymer on magnetite decreased the pore volume to 0.17 cm^2/g and decreased the pore size, also called pore diameter, to 16.30 nm. Lastly, combining chitosan with the nanocomposite significantly decreased the pore volume and pore diameter to 0.09 cm^3/g and 0.003 nm, respectively.

Fe3O4@PEDOT: PSS nanocomposite performance for NaCl and CdCO3 CDI

The chloride ion and toxic cadmium removal were investigated using two electrodes: one which includes chitosan nanosheet (Fe_3O_4@PEDOT: PSS@m-chitosan nanosheets) and one without chitosan nanosheet (Fe_3O_4@PEDOT:

PSS nanocomposite). The former is in the form of nanosheet while the latter is in the form of nanocomposite. The electrochemical sites on Fe_3O_4 are able to intercalate the Na^+ and Cd^- from NaCl and $CdCO_3$, while the PEDOT: PSS has higher electrical conductivity, resulting in higher ion uptake. To fully understand the capacitive deionization of NaCl and $CdCO_3$, changes in specific capacitance before and after CDI and electrosorption capacity for the experiments were studied and discussed. This is because it is not all ions that are electrosorbed are accumulated at the electric double layer regions to generate capacitance in redox active electrodes.

To conduct the CDI experiment, nickel foam current collector, Ag/AgCl reference electrode and both the nanosheet and nanocomposite electrodes were placed in 500ppm NaCl and $CdCO_3$ respectively. The effect of pH (4, 6, 9 and 13), concentration (100, 150, 250, 300 ppm) and cycles (30, 60, 80, 100 cycles) were thoroughly investigated using change in conductivity, change in specific capacitance and electrosorption capacity values. For all variations, CV curves were recorded in the range of -1.2 V to 0 V at scan rate of 100 mV/s, and a maximum current of 30 mA. The quasi-rectangular appearance of the cyclic voltammograms before and after CDI is typical of EDLC capacitors. pH which shows the highest SEC was employed and kept constant for the concentration variation, while the optimum pH and concentrations were kept constant and employed for number of cycles studies.

In the Fe_3O_4@PEDOT: PSS nanocomposite electrode, SEC was highest at the extreme pHs of 4 and 13 due to higher pH gradient driving the Na^+ ions towards the electrodes, while at pH 6 and 9, the salt electrosorption capacity was lower (see Table 3). The higher the concentration, the lower the SEC, due to the fact that ion diffusion to electrodes becomes more difficult as amount of ions to migrate increases against constant current in the CDI experiment, with the CDI of 100 ppm of NaCl showing the highest SEC of 38%. As the number of charge cycle increases, the SEC increased also, with 100 cycles showing the highest SEC of 30.12%. Capacitance change of the electrode before and after CDI seems to correlate with the deionization. The capacitance change decreased with increase in pH, and increased with concentration increases. However, 30 cycles showed the highest capacitance change instead of 100 cycles which shows the highest SEC. Consequently, the salt electrosorption capacity (SEC) shows the extent of CDI better, because some deionized ions that do not contribute to specific capacitance are also present in the solution after CDI experiments. SEC captures not only the ions contributing to capacitance, but it also represents the totality of ions in the solution before and after CDI.

For cadmium ion CDI, the pH gradient factor was not too significant as the SEC decreased with increase in pH. Based on the Pourbaix diagram, Cd^{2+} is more soluble in acidic pH, hence its higher SEC values at pH 4 and 6 (see Table 4). Increase in concentration led to decrease in SEC with 100 ppm Cd^{2+} showing 21% SEC, while increase in CDI cycle led to decreased SEC. As a matter of fact, the Cd^{2+} begin to experience a reverse migration from the electric double layer regions back to the bult solution as CDI cycles increases, same with concentration increase. This is seen in the way the capacitance change decreased as number of cycles increased. In the CDI of Cd^{2+} Fe_3O_4@PEDOT: PSS nanocomposite, capacitance change correlated well with SEC%. In addition, the reverse migration might be due to lack of adequate coulombic forces to hold cadmium ions at the EDLC layers of the nanocomposite electrodes. The CDI of $CdCO_3$ shows lower electrosorption values when compared to that of NaCl because the CO_3^{2-} ions undergoes further interactions in aqueous media after deionization, hence, the conductivity experiment was unable to capture the presence of CO_3^{2-} ions.

Mapping helps to further confirm the species on the electrodes before and after CDI. The mappings confirms the successful migration of sodium and cadmium ions to the Fe_3O_4@PEDOT: PSS nanocomposite electrodes. As the CDI process proceeds, Na^+ and Cd^{2+} ions transfers to the negatively charged electrode at different rates under a constant current charge set-up. Figure 4a and b shows the negative nanocomposite electrode before and after NaCl deionization. Before CDI, the EDX confirms the presence of Fe and S from the PEDOT: PSS and Ni from the current collector. Figure 5 shows the negative nanocomposite electrode after $CdCO_3$ deionization, Cd were confirmed to be trapped. The presence of iron and sulphur showed that the Fe_3O_4@PEDOT: PSS nanocomposite was successfully loaded onto the nickel current collector.

Parameters		Conductivity before	Conductivity after	SEC%	Capacitance before (F/g)	Capacitance after (F/g)	Capacitance change
pH	**4**	1652	1218	26.27	253.65	442.30	188.65
	6	1586	1280	19.29	260.94	343.75	82.81
	9	1531	1224	20.05	353.65	603.65	250
	13	3780	2900	23.28	1061.67	1081.58	20.08
Concentration (ppm)	**100**	3240	2000	38.27	181.55	294.64	113.10
	150	3690	2700	26.82	358.33	393.45	35.12
	250	3930	3070	21.81	388.10	404.17	16.07
	300	4690	3880	17.27	472.62	589.29	116.67
Cycles	**30**	2160	1840	14.81	557.47	865.66	308.19
	60	2040	1670	18.13	755.75	864.94	109.20
	80	1970	1552	21.21	729.89	774.43	44.54
	100	1952	1364	30.12	744.97	956.18	211.21

Table 3. Summary of the capacitive deionization of NaCl using Fe_3O_4@PEDOT: PSS nanocomposite.

Parameters		Conductivity before	Conductivity after	SEC%	Capacitance before (F/g)	Capacitance after (F/g)	Change in capacitance
pH	**4**	1627	1196	26.49	1041.67	2222.22	1180.56
	6	1610	1201	25.40	1194.44	2354.17	1159.72
	9	1564	1257	19.62	1208.33	3250.00	2041.67
	13	3430	3130	8.74	1277.78	2708.33	1430.56
Concentration (ppm)	**100**	4310	3380	21.57	462.50	593.52	131.02
	150	4270	3660	14.28	574.54	619.91	45.37
	250	4440	3870	12.83	503.24	529.17	25.93
	300	4740	4040	14.76	602.78	611.11	8.33
Cycles	**30**	2750	1423	48.25	2218.75	1361.11	857.64
	60	423	264	37.58	1260.42	888.89	371.53
	80	264	228	13.63	805.56	909.72	104.17
	100	228	141	38.15	732.64	930.56	197.92

Table 4. Summary of the capacitive deionization of $CdCO_3$ using Fe_3O_4@PEDOT: PSS nanocomposite.

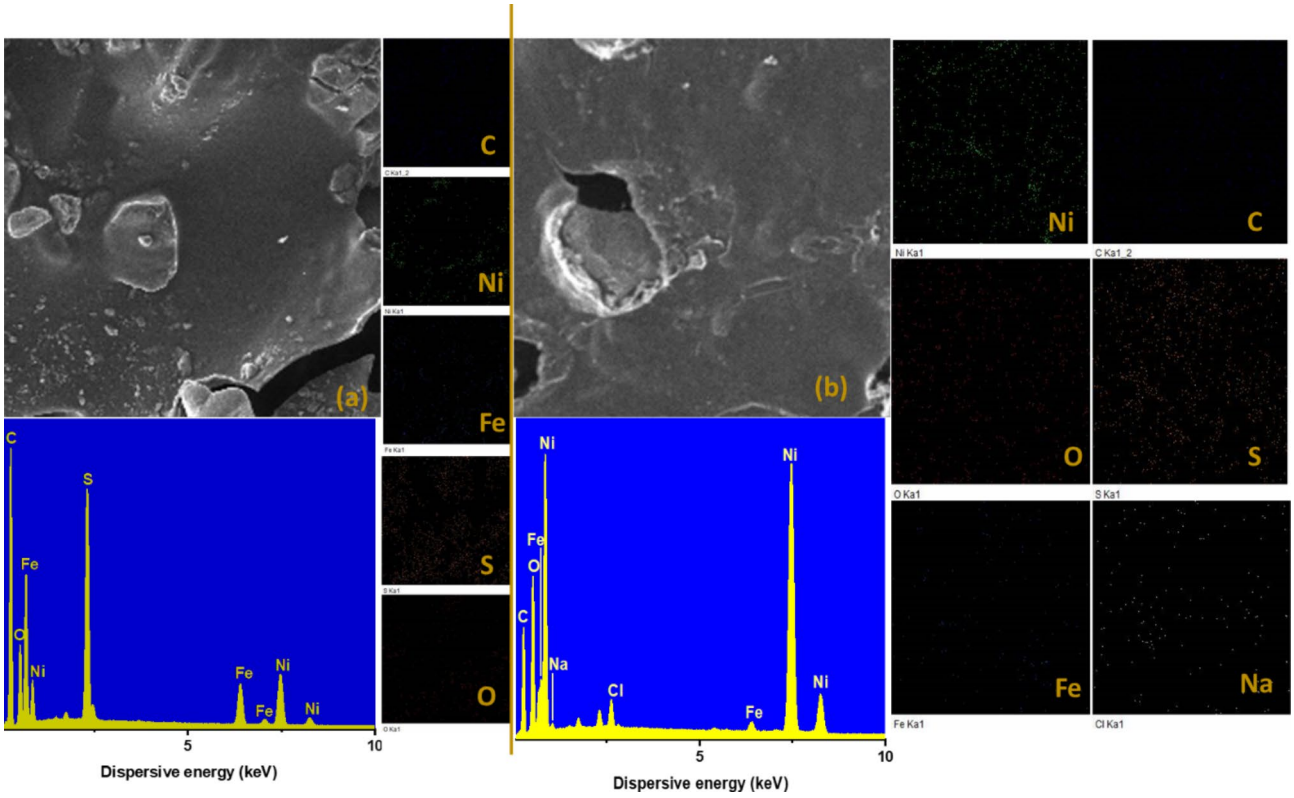

Fig. 4. Fe_3O_4@PEDOT: PSS nanocomposite as negative electrode before (a) and after (b) NaCl deionization.

Fe3O4@PEDOT: PSS modified chitosan nanosheets performance for NaCl and CdCO3 CDI

The electrodes act like a capacitor, storing ions on their surfaces without causing a chemical reaction and this storage process is reversible and energy efficient. The electrochemical sites on Fe_3O_4 are able to intercalate the Na^+ and Cd^{2+}, the PEDOT: PSS has higher electrical conductivity, resulting in higher ion uptake, while the chitosan sheet reduces reverse migration phenomena that was evident in the nanocomposite. To fully account for the capacitive deionization cadmium ions, changes in specific capacitance and conductivity before and after a CDI cycle were used to estimate the electrosorption capacity. The same CDI parameters were varied, and the nanocomposite electrodes were replaced with nanosheet (Fe_3O_4@PEDOT: PSS modified chitosan nanosheets).

The chitosan nanosheets have high surface area and provides support for the Fe_3O_4 thereby improving the salt electrosorption capacities. The chitosan nanosheets are also able to bind with the ions effectively in solutions. In the NaCl deionization with nanosheet, SEC increased with pH and pH gradient was not the only factor driving the CDI and pH 13 shows the highest sodium electrosorption capacity of 70.81% (see Table 5). The SEC increases as the concentration increased from 100 to 150 ppm but starts decreasing around 250 ppm to

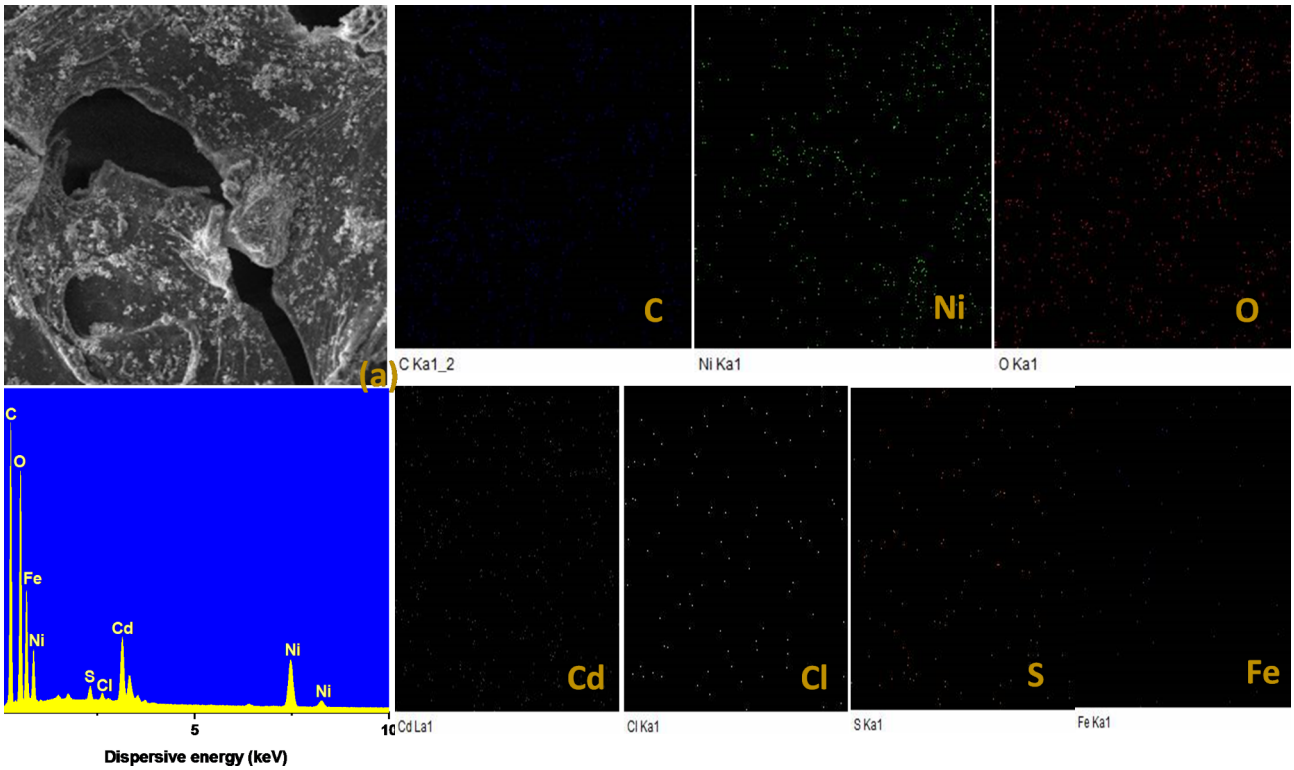

Fig. 5. Fe_3O_4@PEDOT: PSS nanocomposite as negative electrode after $CdCO_3$ deionization.

Parameters		Conductivity before (μ S/cm)	Conductivity after (μ S/cm)	SEC%	Capacitance before (F/g)	Capacitance after (F/g)	Change in Capacitance (F/g)
pH	**4**	1535	988	35.63	145.45	418.56	273.11
	6	1477	362	75.49	123.86	598.48	474.62
	9	1502	503	66.51	175.00	503.41	328.41
	13	4180	1220	70.81	1031.06	1652.76	594.70
Concentration (ppm)	**100**	1862	912	51.02	965.77	1020.83	55.06
	150	2050	577	71.85	653.27	849.70	196.43
	250	2490	991	60.20	1574.40	1358.63	215.77
	300	3550	1030	70.98	654.76	861.61	206.85
Cycles	**30**	2190	937	57.21	249.18	420.75	171.57
	60	1937	416	78.52	354.85	358.93	4.08
	80	1716	301	82.45	331.70	320.26	11.44
	100	1695	485	71.38	339.05	330.34	8.71

Table 5. Summary of the capacitive deionization of NaCl using Fe_3O_4PEDOT: PSS modified chitosan nanosheets.

300 ppm due to reverse migration of Na^+ and loss of coulombic attraction at EDLC regions. Increase in the number of cycles led to increase in section (82% at 80 cycles), at very high cycle, the SEC drops to 71%. In the Cd^{2+} deionization, highest SEC was seen at pH of 4, and it continues to decrease as pH goes to alkaline limits. The SEC increases with concentration too, but starts to decrease at concentration of 250 ppm. The highest Cd^{2+} CDI of 93% was obtained at 100 cycles, confirming no reverse migration of ions from EDLC regions back to bulk media (see Table 6).

When compared to the nanocomposite performance, the nanosheet CDI achieved higher electrosorption at optimum points and at a faster rate. While the nanocomposite CDI took 100 cycles to attain 30% SEC, the nanosheet CDI attained 92% at 30 cycles. In the nanosheet, optimal SEC was reached at 150 ppm for both Na^+ and Cd^{2+} CDI while reverse migration of ions sets in around 250 ppm. However, in the nanocomposite, reverse migration sets in at the initial concentration of 100 ppm. This implies that the nanosheet can hold on to the ions more than the nanocomposite due to the chitosan contribution in the nanosheet. The presence of chitosan also offers high surface area to contribute to the capacitive nature of the nanosheet. The results shows

Parameters		Conductivity before	Conductivity after	SEC%	Capacitance before (F/g)	Capacitance after (F/g)	Change in capacitance
pH	**4**	1914	900	52.97	206.38	300.89	44.52
	6	1954	909	53.48	216.44	127.52	88.93
	9	1894	1308	30.93	218.96	461.41	242.45
	13	3060	2000	34.64	166.67	383.11	216.44
Concentration (ppm)	**100**	39.5	10.94	72.30	0.46	7.41	6.94
	150	8.17	1.31	83.96	5.09	10.65	5.56
	250	9.31	1.97	78.83	6.48	6.38	0.1
	300	53.6	17	68.28	6.48	5.56	0.93
Cycles	**30**	58.6	4.5	92.32	17.50	20.00	2.50
	60	64.5	7.7	88.06	20.83	21.67	0.83
	80	67.7	5.9	91.28	20.83	24.17	3.33
	100	71.9	4.9	93.18	23.50	23.67	0.17

Table 6. Summary of the capacitive deionization of $CdCO_3$ using Fe_3O_4@PEDOT: PSS modified chitosan nanosheets.

Salt	Initial concentration (mgL^{-1})	Desalination capacity ($mg.g^{-1}$)	Electrodes used	Ref
NaCl	500	49.34	Graphene hydrogel	31
	1282	85.94	Mesoporous $FePO_4$ nanospheres	32
	250	3.15	Polyaniline@mesoporous carbon	33
	100	41.3	**This work**	
$CdCl_2$	200	97.5%	Nano-porous carbon aerogel	34
	500	19.3	Graphitic porous carbon nanosheets	35
	1 mM	60	Cu-based metal-organic framework	36
	100	47.8	**This work**	

Table 7. Comparative review of past works with.

good performances even when compared with other literatures on CDI of metal ions from water (see Table 7). In comparison to the conductivity changes, capacitance change was not well correlated to SEC values in the nanosheet like it was in the nanocomposite. Specifically, during cadmium ion CDI, the capacitance changes were very low and does not reflect the high SEC values seen.

Similarly, mapping studies were also carried out for the Fe_3O_4@PEDOT: PSS modified chitosan nanosheets as negative electrodes to confirm the absorption of Na^+ and Cd^{2+}. As CDI processes proceeds, Na^+ and Cd^{2+} ions transfers to the negatively charged electrode and the Cl^- and CO_3^{2-} transfers to the positive electrodes. Figure 6a and b shows the negative nanosheet electrode before and after NaCl deionization. Before CDI, the EDX confirms the presence of Fe from the PEDOT: PSS and Ni from the current collector. Figure 7 shows the negative nanocomposite electrode after $CdCO_3$ deionization, Cd were confirmed to be trapped. The absence of sulphur in the nanosheet shows that the chitosan has covalently bonded with the PEDOT through sulphur linkages.

The mechanism of the CDI proceeds via the migration of the positive sodium and cadmium ions to the Fe_3O_4@PEDOT: PSS modified chitosan nanosheets electrodes as a result of the negative electrostatic pull on the $-NH_2$ units of chitosan and the sulfonate groups on the PEDOT: PSS polymers. Na^+ ions, which are monovalent and smaller, are often eliminated through capacitive deionization, where they are electrostatically drawn to the negatively charged cathode. Cd^{2+}, a divalent ion, can be removed by capacitive adsorption. However, due to its bigger size and higher charge, it can also interact through faradaic processes (charge transfer). The chitosan nanosheets include amine and hydroxyl functional groups, which can chelate metal ions. This chemical binding process enhances ion adsorption, particularly for heavy metals such as Cd^{2+}. Chitosan serves as a chelating agent, binding Cd^{2+} ions to improve removal efficiency. After saturating the electrodes with Na^+ and Cd^{2+} ions, the voltage is reversed in the discharge mode, allowing the ions to desorb back into the water and regenerate the electrodes for future usage.

Conclusion

In summary, a Fe_3O_4@PEDOT: PSS nanocomposite and Fe_3O_4@PEDOT: PSS modified chitosan nanosheets were successfully synthesized and ran at optimal conditions for the capacitive deionization of sodium chloride and cadmium carbonate. It was discovered that the presence of the chitosan nanosheets provides more surface area to the CDI electrodes and allow the process of chloride and toxic cadmium removal to go faster by reducing reverse-migration of ions. In addition, the Fe_3O_4 shows the ability to intercalate well with the Na^+ and Cd^{2+} ions leading to higher electrosorption capacity. PEDOT: PSS has greater electrical conductivity and allows higher uptake of Na^+ and Cd^{2+}. When compared to the nanocomposite performance, the nanosheet CDI achieved

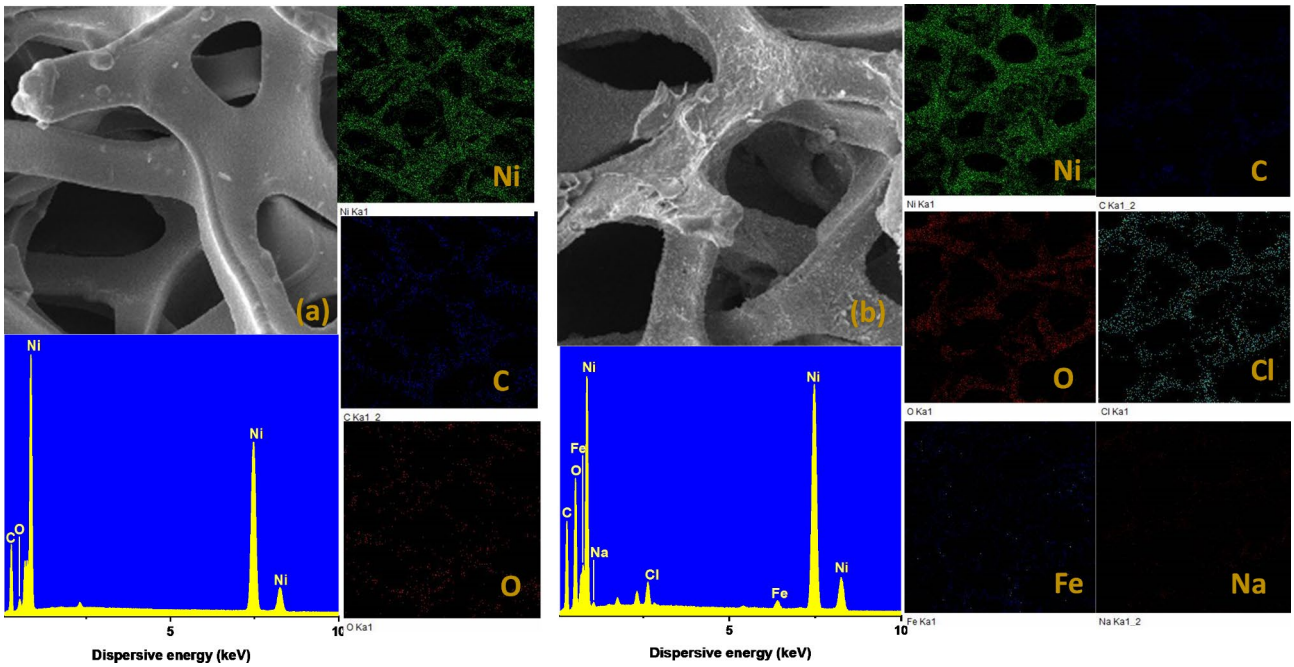

Fig. 6. Negative electrode using Fe_3O_4@PEDOT: PSS modified chitosan nanosheets before and after NaCl deionization.

higher electrosorption at optimum points and at a faster rate. While the nanocomposite CDI took 100 cycles to attain 30% SEC, the nanosheet CDI attained 92% at 30 cycles. In the nanosheet, optimal SEC was reached at 150 ppm for both Na^+ and Cd^{2+} CDI while reverse migration of ions sets in around 250 ppm. However, in the nanocomposite, reverse migration sets in at the initial concentration of 100 ppm.

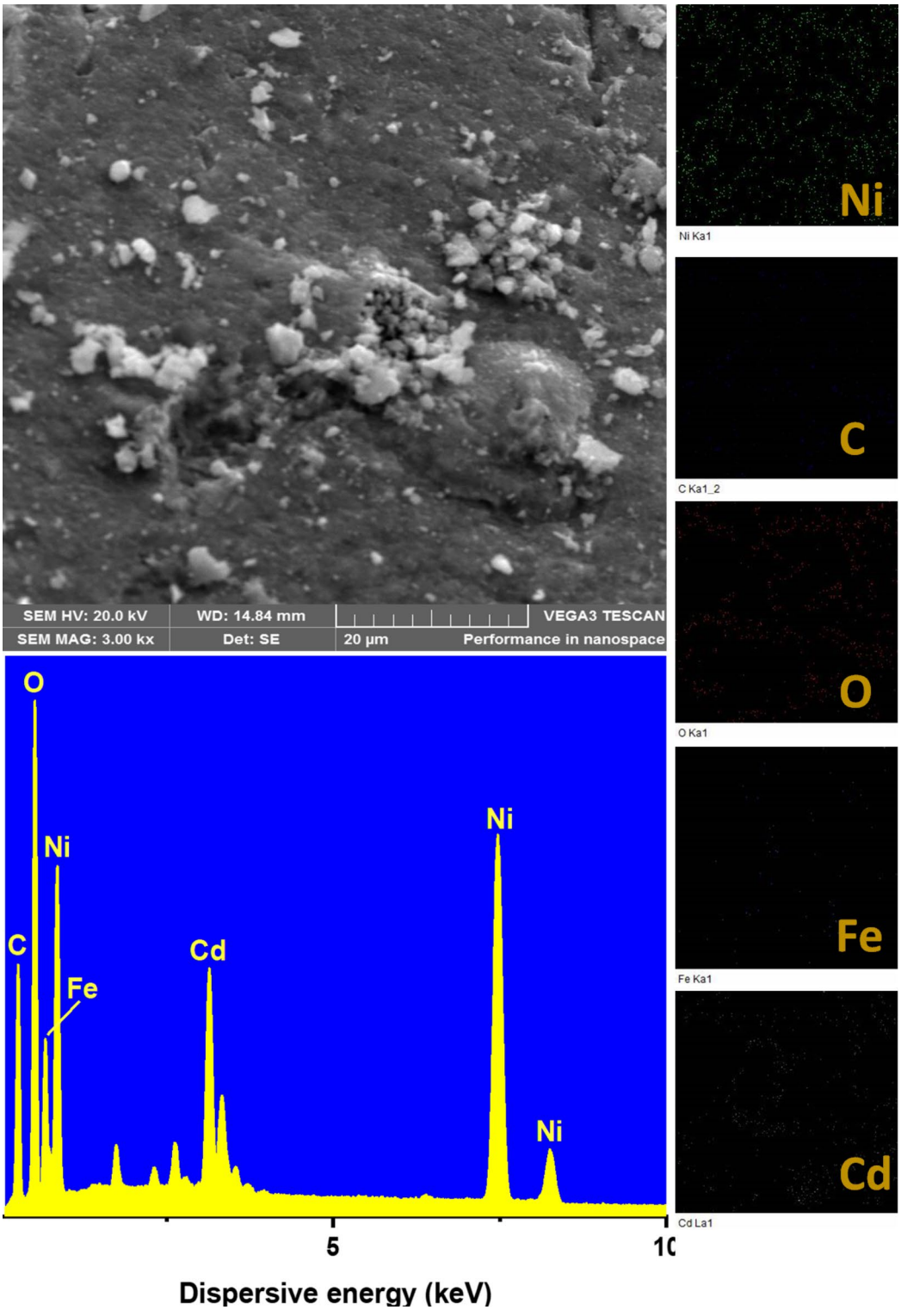

Fig. 7. Positive electrode using Fe_3O_4@PEDOT: PSS modified chitosan nanosheets before and after $CdCO_3$ deionization.

Data availability

The datasets used and/or analysed during the current study available from the corresponding author on reasonable request.

Received: 11 July 2024; Accepted: 28 October 2024
Published online: 15 November 2024

References

1. Bakker, K. The commons versus the commodity: Alter-globalization, anti-privatization and the human right to water in the global south *Glob. Environ. Read.* **187**, 2016 (2007).
2. Boretti, A. & Rosa, L. Reassessing the projections of the world water development report. *NPJ Clean. Water*. **2**, 15 (2019).
3. Zirak, M., Alehdaghi, H., Nodehi, M., Koshki, M. S. & Kazemi, M. Antimicrobial polymer-based nanocomposites for pollutants removal. *Mater. Chem. Horizons*. **2**, 233–248 (2023).
4. Kordbacheh, F. & Heidari, G. Water pollutants and approaches for their removal. *Mater. Chem. Horizons*. **2**, 139–153 (2023).
5. Zare, E. N., Motahari, A. & Sillanpää, M. Nanoadsorbents based on conducting polymer nanocomposites with main focus on polyaniline and its derivatives for removal of heavy metal ions/dyes: A review. *Environ. Res.* **162**, 173–195 (2018).
6. Srivastava, V. et al. Cytotoxic aquatic pollutants and their removal by nanocomposite-based sorbents. *Chemosphere*. **258**, 127324 (2020).
7. Zare, E. N., Lakouraj, M. M. & Masoumi, M. Efficient removal of Pb (II) and Cd (II) from water by cross-linked poly (N-vinylpyrrolidone-co-maleic anhydride)@ eggshell/Fe3O4 environmentally friendly nano composite. *Desalin. Water Treat.* **106**, 209–219 (2018).
8. Sayed, E. T. et al. Recent progress on the application of capacitive deionization for wastewater treatment. *J. Water Process. Eng.* **56**, 104379 (2023).
9. Juve, J. M. A., Christensen, F. M. S., Wang, Y. & Wei, Z. Electrodialysis for metal removal and recovery: A review. *Chem. Eng. J.* **435**, 134857 (2022).
10. Badr, E. A. E., Agrama, A. A. E. & Badr, S. A. E. Heavy metals in drinking water and human health, Egypt. *Nutr. Food Sci.* **41**, 210–217 (2011).
11. Zhao, R., Porada, S., Biesheuvel, P. M. & Van der Wal, A. Energy consumption in membrane capacitive deionization for different water recoveries and flow rates, and comparison with reverse osmosis. *Desalination*. **330**, 35–41 (2013).
12. Jeon, S., Yeo, J., Yang, S., Choi, J. & Kim, D. K. Ion storage and energy recovery of a flow-electrode capacitive deionization process. *J. Mater. Chem. A*. **2**, 6378–6383 (2014).
13. Bolisetty, S., Peydayesh, M. & Mezzenga, R. Sustainable technologies for water purification from heavy metals: Review and analysis. *Chem. Soc. Rev.* **48**, 463–487 (2019).
14. Choi, J., Dorji, P., Shon, H. K. & Hong, S. Applications of capacitive deionization: Desalination, softening, selective removal, and energy efficiency. *Desalination*. **449**, 118–130 (2019).
15. Bharath, G. et al. Enhanced electrochemical performances of peanut shell derived activated carbon and its Fe3O4 nanocomposites for capacitive deionization of Cr (VI) ions. *Sci. Total Environ.* **691**, 713–726 (2019).
16. Kayser, L. V. & Lipomi, D. J. Stretchable conductive polymers and composites based on PEDOT and PEDOT: PSS. *Adv. Mater.* **31**, 1806133 (2019).
17. Houghton, J. I. & Quarmby, J. Biopolymers in wastewater treatment. *Curr. Opin. Biotechnol.* **10**, 259–262 (1999).
18. Shaban, M., Hasanzadeh, M. & Solhi, E. An Fe 3 O 4/PEDOT: PSS nanocomposite as an advanced electroconductive material for the biosensing of the prostate-specific antigen in unprocessed human plasma samples. *Anal. Methods*. **11**, 5661–5672 (2019).
19. Alvand, M. & Shemirani, F. A. Fe 3 O 4@ SiO 2@ graphene quantum dot core-shell structured nanomaterial as a fluorescent probe and for magnetic removal of mercury (II) ion. *Microchim Acta*. **184**, 1621–1629 (2017).
20. Khan, S. & Narula, A. K. Bio-hybrid blended transparent and conductive films PEDOT: PSS: Chitosan exhibiting electro-active and antibacterial properties. *Eur. Polym. J.* **81**, 161–172 (2016).
21. Silva, V. A. J., Andrade, P. L., Silva, M. P. C., Valladares, L. D., Aguiar, J. A. & L. S. & Synthesis and characterization of Fe3O4 nanoparticles coated with fucan polysaccharides. *J. Magn. Magn. Mater.* **343**, 138–143 (2013).
22. Drabczyk, A. et al. Physicochemical investigations of chitosan-based hydrogels containing aloe vera designed for biomedical use. *Mater. (Basel)*. **13**, 3073 (2020).
23. Xiong, S., Zhang, L. & Lu, X. Conductivities enhancement of poly (3, 4-ethylenedioxythiophene)/poly (styrene sulfonate) transparent electrodes with diol additives. *Polym. Bull.* **70**, 237–247 (2013).
24. Queiroz, M. F., Melo, T., Sabry, K. R., Sassaki, D. A. & Rocha, H. Does the use of chitosan contribute to oxalate kidney stone formation? *Mar. Drugs*. **13**, 141–158 (2014).
25. Villegas, V. A. R. et al. Synthesis and characterization of magnetite nanoparticles for photocatalysis of nitrobenzene. *J. Saudi Chem. Soc.* **24**, 223–235 (2020).
26. Kokate, K. K., Bhandarkar, S. E. & Kulkarni, S. A. Synthesis and magnetic properties of poly (3, 4-ethylenedioxythiophene) (PEDOT)/Fe3O4 composites. *IJITR*. **3**, 1925–1929 (2015).
27. Besenhard, M. O. et al. Co-precipitation synthesis of stable iron oxide nanoparticles with NaOH: New insights and continuous production via flow chemistry. *Chem. Eng. J.* **399**, 125740 (2020).
28. Sun, D. C. The synthesis and characterization of electrical and magnetic nanocomposite: PEDOT/PSS–Fe3O4. *Mater. Chem. Phys.* **118**, 288–292 (2009).
29. Issa, B., Obaidat, I. M., Albiss, B. A. & Haik, Y. Magnetic nanoparticles: Surface effects and properties related to biomedicine applications. *Int. J. Mol. Sci.* **14**, 21266–21305 (2013).
30. Liu, X., Hu, Q., Fang, Z., Wu, Q. & Xie, Q. Carboxyl enriched monodisperse porous Fe3O4 nanoparticles with extraordinary sustained-release property. *Langmuir*. **25**, 7244–7248 (2009).
31. Ma, J., Wang, L. & Yu, F. Water-enhanced performance in capacitive deionization for desalination based on graphene gel as electrode material. *Electrochim. Acta*. **263**, 40–46 (2018).
32. Ma, J., Wang, L., Yu, F. & Dai, X. Mesoporous amorphous FePO4 nanosphere@ graphene as a faradic electrode in capacitive deionization for high-capacity and fast removal of NaCl from water. *Chem. Eng. J.* **370**, 938–943 (2019).
33. Yan, C., Zou, L. & Short, R. Polyaniline-modified activated carbon electrodes for capacitive deionisation. *Desalination*. **333**, 101–106 (2014).
34. Marmanis, D. I., Dermentzis, K. I., Christoforidis, A. K. & Ouzounis, K. G. Cadmium removal from aqueous solution by capacitive deionization with nano-porous carbon electrodes. *J. Eng. Sci. Technol. Rev.* **6**, 165–166 (2013).
35. Wang, H. et al. Efficient removal of metal ions by capacitive deionization with straw waste derived graphitic porous carbon nanosheets. *Environ. Sci. Nano*. **7**, 317–326 (2020).
36. Kim, Y. et al. Electrosorption of cadmium ions in aqueous solutions using a copper-gallate metal-organic framework. *Chemosphere*. **286**, 131853 (2022).

Author contributions

Oluwaseyi D. Saliu: Conceptualization, investigation, data curation, methodology, writing-reviewing and editing.Omphemetse Leping : Writing, methodology, data curation, methodology, software.Tunde L. Yusuf: Software, plottings and analysisAdewale G. Adeniyi : Reviewing, editing, interpretation.James Ramontja: Conceptualization, project administration, supervision, validation, funding acquisition.

Declarations

Competing interests
The authors declare no competing interests.

Additional information
Supplementary Information The online version contains supplementary material available at https://doi.org/10.1038/s41598-024-77931-4.

Correspondence and requests for materials should be addressed to O.D.S. or J.R.

Reprints and permissions information is available at www.nature.com/reprints.

Publisher's note Springer Nature remains neutral with regard to jurisdictional claims in published maps and institutional affiliations.